Potassium-Induced Emission Enhancement of Bovine Serum Albumin-Stabilized Red-Emitting Au Nanoclusters: Mechanism and Application to Blood Plasma

Achmad Hidayat
Shibaura Institute of Technology
Nicole Wawrzyniak
Lodz University of Technology
Adam Domanski
Lodz University of Technology
Yutaka Shibata
Tohoku University
Akiko Hori
Shibaura Institute of Technology
Shuichi Hashimoto
NIT Gunma College
Izabela Rzeznicka (izabela@shibaura-it.ac.jp)
Shibaura Institute of Technology

Research Article

Keywords: Bovine serum albumin, Au25 nanocluster, emission enhancement, potassium

Posted Date: December 7th, 2021

DOI: https://doi.org/10.21203/rs.3.rs-1120374/v1

Abstract

Aggregation-induced emission (AIE) enhancement is attractive for bioimaging as it offers higher quantum yields (QYs) from fluorophores via modulation of their immediate environment. Fluorophores with high QYs are essential probes for investigating the spatiotemporal distribution of physiologically important metal ions such sodium and potassium. Potassium ions are vital for normal function of living organisms. The research reported here evaluates the emission intensity of the bovine serum albumin-stabilized red-emitting gold nanoclusters (BSA-rAuNCs) upon uptake of K^+. The integrated sphere method was used to determine the absolute QYs and a custom-built fluorescence setup recorded the emission spectra of BSA-rAuNCs. Enhancement of emission intensity was observed upon increasing K^+ concentration, within the physiological concentration range of 0 - 150 mM. The emission enhancement was correlated with the particle size and charge analysis. Aggregation of BSA-rAuNCs was found to be responsible for the observed emission enhancement. The QY of BSA-rAuNCs in bovine blood plasma was found to be four times lower than corresponding QY in water.

Introduction

The small size and tunable emission properties of gold nanoclusters (AuNCs) have triggered research interest in the potential applications of AuNCs in bioimaging, biosensing and cancer therapy [1–3]. The emission quantum yield (QY) and stability of AuNCs depends on the nature of stabilizing molecules and the properties of the solvents used with them [4]. Thiols have often been used to stabilize AuNCs due to the strong affinity of sulphur for gold. Stabilization with dendrimer molecules resulted in much higher QYs, but an increased ensemble size and low compatibility with aqueous solutions have been a major obstacle to *in vivo* imaging using highly emissive AuNCs [5]. Protein scaffolds offer another biocompatible way to stabilize AuNCs [6]. Among various proteins, albumins have been widely used due to their known ion- and drug-binding properties. Recently, our group showed that bovine serum albumin (BSA) can hold several Au_8NCs. BSA-encapsulated blue-emitting Au_8NCs were found to exhibit two-photon absorption which could be advantageous for *in-vivo* imaging [7]. The interaction of BSA-Au_8NCs with lipid membranes provided insights into the conformation changes that BSA-Au undergoes when in contact with lipid membranes [8]. Several research groups demonstrated applications of conjugated BSA-AuNCs in fluorescent contrast imaging of living cells, including cancer [9–11]. From the nanomaterial safety standpoint the renal clearance and toxicity of red-emitting AuNCs have also been evaluated [12].

Albumins act as transport proteins which bind to various ligands and ions thus, in principle, BSA-AuNCs could be used to mark the distribution of metal ions inside cells, and their movement across the cell membrane. Potassium ions are important for normal cell functioning so being able to visualize their uptake and release is very useful for investigating cell metabolism. However, few potassium-specific fluorescent probes have been developed so far. Benzofuran isopthalate (PBFI) was the first commercially available probe for imaging spatiotemporal potassium distribution within cells [13]. However, it suffered from low selectivity in the presence of sodium ions and poor intracellular loading [14, 15]. Consequently,

fluorophores conjugated with ion-size specific ionophores have been synthesized, improving selectivity and cell membrane permeability through modification with acetoxymethyl (AM) esters. Asante potassium green (APG) probes are commercially available for intracellular potassium imaging. However, a drawback of APG-AM probes is their low QY and requirement for esterase enzymes to be present for fluorescence to occur. These probes also require a long incubation time in order to obtain a discernible fluorescent signal. The QY of the APG-2AM probe in water is negligible. In addition it was shown that fluorescence reached saturation at a K^+ concentration of 80 mM, thus the probe is not able to respond to K^+ changes at physiological intracellular potassium concentrations, which is 140-150 mM [15]. Recently, genetically encoded fluorescence resonant energy transfer (FRET) probes were bioengineered and used for imaging intracellular potassium ion concentration with high selectivity and fluorescence intensity [16]. The difficulty in using these bioengineered probes lies in the time required for their synthesis and their high cost. The reported high affinity of FRET probes for potassium ions is also far from physiological intracellular potassium concentration.

Aggregation-induced emission (AIE) is a photophysical process that has been used in recent years to turn non- or weakly-luminescent probes into highly emissive probes [17]. For example, binding of several fluorescent probes with albumins yielded a huge enhancement of fluorescence QYs [17, 18]. This enhancement was attributed to restricted intramolecular motions (rotations and vibrations) in the protein-fluorescence probe adduct. Consequently, fluorogens with AIE have emerged as a new class of fluorescent probes for studying spatiotemporal ion distribution. Albumins were found to provide the necessary environment for many fluorescent probes to enhance their QYs.

The lack of small and cost-effective fluorescent probes with high QY for potassium imaging prompted us to evaluate the emission QY of BSA-stabilized red-emitting AuNCs (BSA-rAuNCs) in the presence of potassium ions. The emission intensity was evaluated in response to potassium ions within physiological concentration range (1.5 mM -150 mM). The observed emission QY enhancement was correlated with the particle size and charge analysis. Based on these studies an enhancement mechanism has been proposed.

Experimental

Reagents and materials

Potassium chloride (KCl, ≥ 99.99%) and gold (III) chloride hydrate ($HAuCl_4 \times 3H_2O$, 99.99%), were purchased from Sigma-Aldrich. Bovine serum albumin (BSA, fatty acid/IgG/protease-free, 98% and sodium hydroxide (NaOH) were purchased from Fujifilm Wako Pure Chemical Corporation. Bovine blood in sodium citrate was purchased from Rockland Immunochemicals, Inc. (Limerick, PA, USA). Cellulose membrane was purchased from Spectra/Por. All chemicals were used without further purification. Ultrapure water with a specific resistance of 18.2 MΩ, and total organic carbon below 3 ppm was used throughout the experiments. A 3 M stock solution of KCl was prepared by dissolving 5.86 g KCl in 50 ml ultrapure water. Further dilutions were performed as appropriate to obtain desired KCl concentrations.

Synthesis of BSA-rAuNCs

BSA-rAuNCs were prepared according to the previously reported procedure [19]. In brief, aqueous solution of $HAuCl_4$ (10 mM, 10 ml) and BSA (50 mg/ml, 10 ml) were mixed under vigorous stirring conditions. After stirring at 750 rpm for 10 minutes at 37°C, NaOH solution (1 M) was added to adjust pH to 12. Then, the reaction was allowed to proceed at 37°C for 12 h at 700 rpm. After cooling, the resultant brown solution was dialyzed against ultrapure water using cellulose membrane (MWCO = 30 kDa), and stored in the dark at 4**°**C. In the experiments, 10 µl of AuNCs solution was mixed with 1990 µl of KCl solutions within the physiological concentration range.

Luminescence studies of BSA- rAuNCs

Luminescence spectra were acquired using a commercial spectrofluorometer (FP-6500 JASCO), and a custom-built fluorescence set-up. Emission spectra recorded at the FP-6500 were taken using a scan speed of 200 nm/min. A rectangular suprasil quartz cell (10 mm path, FP-1003 JASCO) was used as the sample container.

The custom-built fluorescence set-up consisted of a green laser diode (532 nm, 0.06 W/cm^2, JMS-30RB, Light Vision Technologies) used as the excitation source. Iris diaphragms were used for optical alignment and for regulating the intensity of the incident beam. Band-pass filters (Semrock, LP03-532RE) were used to pass beam wavelengths within a 532 nm range and to reject (attenuate) frequencies outside that range. Neutral-density (ND) filters were used to reduce laser beam intensity. A rectangular suprasil quartz cell (10 mm path, FP-1003 JASCO) was used as the sample container. The cuvette was mounted in the black cuvette holder (10 × 10 mm, Newport) to maintain the same geometrical conditions during measurements with different samples. Emission spectra were acquired with a spectrograph (Acton SP-150, 300g/mm gratings) and liquid N_2-cooled CCD camera (Princeton Instruments, Spec10:256E) having dark current of 3 electrons/scan. Wavelength calibration before each measurement was done using a neon lamp. The overall spectral resolution of the system is 0.3 nm. For each measurement, the sample was continuously stirred during spectrum acquisition, to avoid thermal gradients.

All acquired emission spectra were further corrected for the wavelength-dependent sensitivity of the detection system using 4-dimethylamino-4'-nitrostilbene (4,4’-DMANS) dye dissolved in *o*-dichlorobenzene (Sigma Aldrich, ≥99.8%) which has emission in the same wavelength region as the BSA-rAuNCs. The maximum wavelength of 4,4’-DMANS emission was 700 nm, not 723 nm, [20]. and corrected emission spectra were taken from Suzuki *et al.*[21].

Emission QY was measured using an absolute photoluminescence quantum yield system (Hamamatsu C9920-01) with a photonic multichannel analyzer (PMA-12) and BT-CCD image sensor (C10027-01) having dark current of 32 electrons/scan (at -15°C). QYs were calibrated using quinine sulphate in 0.1 N H_2SO_4 as a standard. Its QY was estimated to be 0.57 at λ_{ex} = 350 nm, consistent with the values found in the textbook [20].

Zeta potential and hydrodynamic radius

Zeta potential and hydrodynamic radius were measured using DelsaMax Pro (Beckman Coulter, Indianapolis, USA). The instrument implements the massively parallel phase analysis light scattering (MP-PALS) technique, as a first-principal electrophoretic mobility measuring method. Since molecular hydrodynamic radius of BSA-rAuNCs is much larger than the Debye length, the zeta potential was derived from Smoluchowski's equation. The hydrodynamic radius was calculated from the Stokes-Einstein equation using diffusion coefficient obtained from the correlation function.

DelsaMax Pro flow cell and disposable cuvettes (made of poly(methyl methacrylate)) were used for zeta potential and hydrodynamic radius measurements, respectively. Samples were prepared by diluting BSA-rAuNCs (25 times, to ~2 mg/mL) into solutions with desired KCl concentration. Diode pumped solid state laser (532 nm, 50 mW) was used as a light source for all measurements.

Results And Discussion

Emission spectra of BSA-rAuNCs

Figure 1 shows a photoexcitation spectrum acquired on a dialyzed sample with pH = 9.6 (left spectrum). The spectrum shows a main peak at 527 nm and a shoulder at 500 nm. On the right side of the graph, emission spectra upon excitation at 500 and 527 nm are shown. At both excitation wavelengths, a broad peak is observed with the maximum at 670 nm for 500 nm excitation and a peak at 678 nm for 527 nm. Such excitation wavelength-dependent shift in the emission spectra was observed for BSA-rAuNCs as well as for BSA-AgNCs [22, 23]. Some authors attributed the shift to the presence of NCs with different size, and some to the presence of Au(I) oligometric structures.

Emission origin of BSA-rAuNCs

A synthesis protocol, proposed by Xie. *et al.* is widely used to prepare BSA-rAuNCs. In this protocol, $HAuCl_4$ is mixed with BSA while the pH of the mixture is raised to 12 [19]. For a long time, the red emission of solutions prepared using the protocol has been attributed to the presence of Au_{25}NCs in BSA scaffold. Recently, however, the origin of the red-emission has been disputed. It was earlier proposed that the Au^{3+} ions of the gold precursor are first reduced to Au (0) by the hydroxyl group of tyrosine residues of BSA, since required pH was close to the pKa of tyrosine (10.46) [19]. Dixon *et al.* investigated the occurrence of the red emission in the pH range from neutral to basic [24]. Their studies revealed that the onset of the red emission occurs at pH = 9.7, which is below pKa of tyrosine. In another paper, the same authors have debated assignment of the red emission to Au_{25}NCs, nucleated at the single-site [25]. This assignment to Au_{25}NCs was based on results obtained using the matrix-assisted laser desorption ionization time-of-flight (MALDI-TOF) technique [19]. The method can only reveal the mass increase of BSA upon the uptake of Au ions and provides information on the total number of Au atoms but not on the cluster size or their distribution inside protein. Indeed, our studies revealed a linear dependence on the

m/z with $HAuCl_4$ concentration, and a time-dependent *m/z* increase [7, 26]. Since crystal structure of BSA-rAuNCs is unknown, the MALDI results cannot be definitely used to assign the origin of the red emission to Au_{25}NCs.

These earlier studies prompted renewed investigation aimed at identification of reducing residues and the origin of the red emission. Recently, a thorough systematic study was published by Hsu *et al.* who investigated the NCs capping moieties of BSA [27]. A detailed analysis of mass spectra under enzyme and disulfide bond digestion revealed that the red-emitting core fraction contains Au and cysteine residues. The disulfide pairs C75-C91/C90-C101 in domain IA, C315-C360/C359-C368 in domain IIB, and C513-C558/C557-C566 in domain IIIB were identified as capping sites of red-emitting AuNCs. By mapping 97% of the BSA sequence, multiple aminoacid oxidation sites have been identified. BSA-rAuNCs were extensively oxidized at multiple methionine and cysteine sites and moderately oxidized at histidine sites. A small percentage of tyrosine residues were found to be oxidized. Based on these studies it has been proposed that methionines and cysteines are responsible for the reduction of Au ions. BSA has only one free cysteine residue. The other 17 cysteines form disulfide bridges. The primary nucleation sites are likely the free cysteine and cysteines freed from their disulfide bond via hydrolysis in alkaline solutions. It has been shown that uncoordinated Au atoms are efficient in cleaving disulfide bonds [28]. At pH 12, disulfide bonds cleavage along with the BSA conformation change from N- to A-form favors nucleation [29]. Nucleation process involves formation of S-Au-S staple motifs. Such motifs are well known in the chemistry of thiols with Au [30]. According to molecular dynamics (MD) simulation, Au clusters grow close to cysteine sites across all three domains of BSA [31]. The domains IIB and IA were reported to accommodate large clusters composed of more than 12 gold atoms. The widely observed excitation wavelength-dependent shift in the emission spectra is in line with the presence of AuNCs of different sizes across different regions of BSA [32].

The majority of X-ray photoelectron spectroscopy (XPS) studies for the red-emitting BSA-AuNCs show that the observed Au (4f) binding energy falls into values between Au (I) and Au (0) (Au (I)-S at ~86.0 eV and Au(0) at 83.8 eV) [33–35]. Recently, Wu *et al.* used synchrotron-based X-ray absorption fine structure (XAFS) spectroscopy to resolve interactions between few-atom Au clusters and BSA [36]. In-depth analysis confirmed the presence of interlocked gold-thiolate (RS-Au-SR) ring structures, which slowly develop over the course of the synthesis. The FT-XAFS analysis showed no significant Au (0) core structure. Fitting of spectra in the Au-S region yielded a coordination number of 2.1 and a bond length of 2.31 (2) Å [37]. The authors indicated that there *are inter-molecular aurophilic*, Au(I)-Au(I), interactions among the SR-Au(I)-SR structures of BSA-rAuNCs complex.

In order to understand the origin of the emission, Chevrier *et al.* used enzyme digestion to show a correlation between intensity of the red emission and rigidity of BSA.[37]. The rigidity is attributed to interlocking Au(I)-SR moieties that also enhance formation of Au(I)-Au(I) bonds. High rigidity resulted in strong emission. The effect is well-known to enhance the luminescence of Au complexes composed of aurophilic oligomers [38, 39]. Such oligomeric structures exhibit a microsecond-long photoluminescence decay component, observed also in this study (Fig. S1&S2) [34].

Figure 2 shows the sensitivity-corrected emission spectrum recorded with the custom-built set-up using a liquid N_2-cooled CCD camera. The spectrum shows a main peak at 675 nm and a shoulder at 650 nm. Wu *et al.* assigned the shorter-wavelength shoulder emission to the ligand-to-metal charge transfer (LMCT) transitions of Au-S moieties [36]. The main emission at ~670 nm has been assigned to the ligand-to metal-metal charge transfer (LMMCT) transitions that are due to the aurophilic Au(I)-Au(I) interaction [36, 40].

Potassium-induced emission enhancement of BSA-rAuNCs

Figure 3 shows selected emission spectra of the BSA-rAuNCs in the presence of increasing KCl concentration acquired with the custom-built fluorescence set-up. The spectra were acquired after 20 min stabilization and were normalized to the emission spectra at 0 mM KCl. Light emission is found to increase with increasing KCl concentration.

The integrated and normalized intensities of the emission spectra for KCl concentrations of 0, 1.5, 5, 10, 50, 100 and 150 mM KCl are plotted in Fig. 4. The intensity of emission sharply increases within 1-15 mM KCl concentration region and levels off at around 50 mM.

In order to understand the observed emission enhancement of the samples, the size and charge of particles present in the solutions were evaluated. Table 1 summarizes the results and the results of QY measurements for a given KCl concentration. The observed size of prepared BSA-rAuNCs is around 9.6 nm, consistent with the previous dynamic light scattering (DLS) and small-angle X-ray scattering (SAXS) results. At pH 9.5, (pH after dialysis) the zeta potential is −37mV and QY is 13%.

Table 1
Hydrodynamic diameter, zeta potential, and quantum yield of the BSA-rAuNCs in the presence of KCl.

[KCl] (mM)	Hydrodynamic diameter (nm)	Zeta potential (mV)	Quantum yield (%)
0	9.6 ± 1.3	-36.7 ± 5.4	13 ± 0.3
1.5	27.1 ± 2.7	-15.0 ± 4.8	
15	37.3 ± 2.7	-6.2 ± 2.5	
150	49.6 ± 6.9	-1.6 ± 1.7	21± 1.4

Upon KCl addition, the charge becomes less negative and reaches an almost neutral value at KCl concentration of 150 mM, which corresponds to typical intracellular potassium concentration. The size of assemblies formed in the solution increases to around 50 nm at 150 mM KCl. Aggregation at high KCl concentration is caused by charge neutralization and the salting-out effect in which the thickness of hydration layer on protein decreases.

Aggregation-induced emission enhancement of BSA-rAuNCs

Au(I)–thiolate complexes exhibit strong luminescence emission by the mechanism of aggregation-induced emission [34, 36]. The origin of strong emission has been attributed to the aurophilic interactions [39]. According to the EXAFS spectra analysis, luminescence intensity of glutathione-stabilized AuNCs was proportional to the degree of Au(I)-Au(I) bonds [36]. Recent transmission electron miscopy (TEM) images of BSA-rAuNCs, after a prolonged incubation, show the presence of long chains with triangular-shaped side chains [41]. It is likely that the backbone chains in the images correspond to Au(I)-Au(I) linear chains and the side chains are Au(I)-(SR) residues. Francos *et al*. found that addition of sodium and potassium into solutions containing Au-SG NCs enhances their emission via formation of inter-cluster electrostatic linkages that promote formation of aurophilic interactions [42].

In view of the emerging new facts about Au-SG NCs, the enhancement of the emission of BSA-rAuNCs in the presence of KCl observed in this work can be explained as follows. At low KCl concentrations, BSA molecules containing various amount of Au atoms are far apart and protected by water molecules forming a hydration shield (HS) of some thickness (Fig. 5a). Upon increasing KCl concentration, the positive ions bind to carboxylate groups of aminoacids, with Cl^- ions also binding to Au atoms. At high KCl concentrations, BSA molecules start to aggregate due to the salting-out effect which causes thinning of hydration layer on protein. In the aggregated protein assemblies, the interprotein aurophilic gold bridges form that restrict BSA rotational freedom resulting in the enhanced luminescence (Fig. 5b).

Emission of BSA-rAuNCs in bovine blood plasma

Potential application of AuNCs in cell imaging have been demonstrated in recent years thus emission intensity of BSA-rAuNCs was also investigated upon mixing with bovine blood plasma [11, 43]. The emission spectrum acquired with the custom-built fluorescence set-up is shown in Fig. 6 along with the spectrum obtained in water.

In blood plasma, the maximum wavelength of emission is shifted towards longer wavelength, and intensity is lower than in water. At 532 nm excitation the QY was around 3.33% but was decreasing with time, suggesting changes of cluster size and its chemical morphology due to interaction with blood plasma proteins.

Conclusions

The emission intensity of the red-emitting BSA-AuNCs was investigated as function of KCl within concentration range encountered under physiological conditions (0-150 mM). Increasing of potassium ion concentration resulted in the enhancement of light emission. This increase was attributed to intramolecular aggregation via Au(I)-Au(I) bond formation. The absolute QY of BSA-rAuNCs measured with the integrated sphere was 13%. When NCs are mixed with the bovine plasma, the QY is only 3%. This

small QY is insufficient for *in-vivo* imaging. Thus, application of the NCs in bioimaging should be reconsidered in view of new facts that are emerging about BSA-rAuNCs aggregation, reactivity and poor renal clearance [12].

Declarations

Conflicts of interest

There are no conflicts to declare.

References

1. Shang L, Dong S, Nienhaus GU (2011) Ultra-small fluorescent metal nanoclusters: Synthesis and biological applications. Nano Today 6: 401-418. https://doi:10.1016/j.nantod.2011.06.004.
2. Tan X, Jin R (2013) Ultrasmall metal nanoclusters for bio-related applications. Wires Nanomed. Nanobi. 5: 569-581. https://doi:10.1002/wnan.1237.
3. Peralta DV, He J, Wheeler DA, Zhang JZ, Tarr MA (2014) Encapsulating gold nanomaterials into size-controlled human serum albumin nanoparticles for cancer therapy platforms. J. Microencaps. 31: 824-831. https://doi:10.3109/02652048.2014.940012.
4. Negishi Y, Nobusada K, Tsukuda T (2005) Glutathione-protected gold clusters revisited: Bridging the gap between gold(I)−thiolate complexes and thiolate-protected gold nanocrystals. J. Am. Chem. Soc. 127: 5261-5270. https://doi:10.1021/ja042218h.
5. Zheng J, Petty JT, Dickson RM (2003) High quantum yield blue emission from water-soluble Au_8 nanodots. J. Am. Chem. Soc. 125: 7780-7781. https://doi:10.1021/ja035473v.
6. Chevrier DM, Chatt A, Zhang P (2012) Properties and applications of protein-stabilized fluorescent gold nanoclusters: Short review. J. Nanophoton. 6(1): 064504. https://doi:10.1117/1.jnp.6.064504.
7. Kindi HA, Mohamed A, Kajimoto S, Zhanpeisov N, Horino H, Shibata Y, Rzeznicka II, Fukumura H (2018) Single bovine serum albumin molecule can hold plural blue-emissive gold nanoclusters: A quantitative study with two-photon excitation. J. Photochem. Photobiol. A: Chem. 357: 168-174. https://doi:https://doi.org/10.1016/j.jphotochem.2018.02.029.
8. Putra RP, Ikumura Y, Horino H, Hori A, Rzeznicka I (2019) Adsorption and conformation of bovine serum albumin with blue-emitting gold nanoclusters at the air/water and lipid/water interfaces. Langmuir 35: 16576-16582. https://doi:10.1021/acs.langmuir.9b02831.
9. Jun W, Bingbo Z (2018) Bovine serum albumin as a versatile platform for cancer imaging and therapy. Curr. Med. Chem. 25: 2938-2953. https://doi:https://dx.doi.org/10.2174/0929867324666170314143335.
10. Zhang P, Yang XX, Wang Y, Zhao NW, Xiong ZH, Huang CZ (2014) Rapid synthesis of highly luminescent and stable Au_{20} nanoclusters for active tumor-targeted imaging *in vitro* and *in vivo*. Nanoscale 6: 2261-2269. https://doi:10.1039/c3nr05269a.

11. Li H, Li H, Wan A (2020) Luminescent gold nanoclusters for in vivo tumor imaging. Analyst 145: 348-363. https://doi:10.1039/C9AN01598A.
12. Zhang XD, Wu D, Shen X, Liu PX, Fan FY, Fan SJ (2012) In vivo renal clearance, biodistribution, toxicity of gold nanoclusters. Biomaterials 33: 4628-4638. https://doi:10.1016/j.biomaterials.2012.03.020.
13. Jezek P, Mahdi F, Garlid KD (1990) Reconstitution of the beef heart and rat liver mitochondrial K+/H+ (Na+/H+) antiporter. Quantitation of K+ transport with the novel fluorescent probe, PBFI. J. Biol. Chem. 265: 10522-10526. https://doi:10.1016/S0021-9258(19)47321-3.
14. Minta A, Tsien RY (1989) Fluorescent indicators for cytosolic sodium. J. Biol. Chem. 264: 19449-19457. https://doi:10.1016/S0021-9258(19)47321-3.
15. Rimmele TS, Chatton JY (2014) A novel optical intracellular imaging approach for potassium dynamics in astrocytes. PLOS ONE 9: e109243. https://doi:10.1371/journal.pone.0109243.
16. Shen Y, Wu SY, Rancic V, Aggarwal A, Qian Y, Miyashita SI, Ballanyi K, Campbell RE, Dong M (2019) Genetically encoded fluorescent indicators for imaging intracellular potassium ion concentration. Commun. Biol. 2: 18. https://doi:10.1038/s42003-018-0269-2.
17. Mei J, Leung NLC, Kwok RTK, Lam JWY, Tang BZ (2015) Aggregation-induced emission: Together we shine, united we soar! Chem. Rev. 115: 11718-11940. https://doi:10.1021/acs.chemrev.5b00263.
18. Barbero N, Butnarasu C, Visentin S, Barolo C (2019) Squaraine dyes: Interaction with bovine serum albumin to investigate supramolecular adducts with aggregation-induced emission (AIE) properties. Chem-Asian J. 14: 896-903. https://doi:10.1002/asia.201900055.
19. Xie J, Zheng Y, Ying JY (2009) Protein-directed synthesis of highly fluorescent gold nanoclusters. J. Am. Chem. Soc. 131: 888-889. https://doi:10.1021/ja806804u.
20. Lakowicz JR (2011) Principles of fluorescence spectroscopy. Springer US, Baltimore.
21. Suzuki K, Kobayashi A, Kaneko S, Takehira K, Yoshihara T, Ishida H, Shiina Y, Oishi S, Tobita S (2009) Reevaluation of absolute luminescence quantum yields of standard solutions using a spectrometer with an integrating sphere and a back-thinned CCD detector. Phys.Chem.Chem.Phys. 11: 9850-9860. https://doi:10.1039/B912178A.
22. Wen X, Yu P, Toh YR, Ma X, Huang S, Tang J (2013) Fluorescence origin and spectral broadening mechanism in atomically precise Au_8 nanoclusters. Nanoscale 5: 10251-10257. https://doi:10.1039/c3nr03015f.
23. Diez I, Ras RHA, Kanyuk MI, Demchenko AP (2013) On heterogeneity in fluorescent few-atom silver nanoclusters. Phys.Chem.Chem.Phys. 15: 979-985. https://doi:10.1039/c2cp43045b.
24. Dixon JM, Egusa S (2018) Conformational change-induced fluorescence of bovine serum albumin–gold complexes. J. Am. Chem. Soc. 140: 2265-2271. https://doi:10.1021/jacs.7b11712.
25. Dixon JM, Egusa S (2019) Kinetics of fluorophore formation in bovine serum albumin–gold complexes. J. Phys. Chem. C 123: 10094-10100. https://doi:10.1021/acs.jpcc.9b00413.

26. Chaudhari K, Xavier PL, Pradeep T (2011) Understanding the evolution of luminescent gold quantum clusters in protein templates. ACS Nano 5: 8816-8827. https://doi:10.1021/nn202901a.
27. Hsu Y, Hung MJ, Chen Y, Wang T, Ou Y, Chen S (2019) Identifying reducing and capping sites of protein-encapsulated gold nanoclusters. . Molecules 2019: 1630. https://doi:10.3390/molecules24081630.
28. Rzeźnicka II, Lee J, Maksymovych P, Yates JT (2005) Nondissociative chemisorption of short chain alkanethiols on Au(111). J. Phys. Chem. B 109: 15992-15996. https://doi:10.1021/jp058124r.
29. Curvale RA (2009) Buffer capacity of bovine serum albumin (BSA). J. Argent. Chem. Soc 97: 174-180.
30. Jiang DE, Tiago ML, Luo W, Dai S (2008) The “staple” motif: A key to stability of thiolate-protected gold nanoclusters. J. Am. Chem. Soc. 130: 2777-2779. https://doi:10.1021/ja710991n.
31. Simms GA, Padmos JD, Zhang P (2009) Structural and electronic properties of protein/thiolate-protected gold nanocluster with “staple” motif: A XAS, L-DOS, and XPS study. J. Chem. Phys. 131: 214703. https://doi:10.1063/1.3268782.
32. Abeyasinghe N, Kumar S, Sun K, Mansfield JF, Jin R, Goodson T (2016) Enhanced emission from single isolated gold quantum dots investigated using two-photon-excited fluorescence near-field scanning optical microscopy. J. Am. Chem. Soc. 138: 16299-16307. https://doi:10.1021/jacs.6b07737.
33. Kawasaki H, Hamaguchi K, Osaka I, Arakawa R (2011) Ph-dependent synthesis of pepsin-mediated gold nanoclusters with blue green and red fluorescent emission. Adv. Funct. Mater. 21: 3508-3515. https://doi:10.1002/adfm.201100886.
34. Luo Z, Yuan X, Yu Y, Zhang Q, Leong DT, Lee JY, Xie J (2012) From aggregation-induced emission of au(i)–thiolate complexes to ultrabright Au(0)@Au(I)–thiolate core–shell nanoclusters. J. Am. Chem. Soc. 134: 16662-16670. https://doi:10.1021/ja306199p.
35. Le Guével X, Hötzer B, Jung G, Hollemeyer K, Trouillet V, Schneider M (2011) Formation of fluorescent metal (Au, Ag) nanoclusters capped in bovine serum albumin followed by fluorescence and spectroscopy. J. Phys. Chem. C 115: 10955-10963. https://doi:10.1021/jp111820b.
36. Wu M, Zhao J, Chevrier DM, Zhang P, Liu L (2019) Luminescent Au(I)–thiolate complexes through aggregation-induced emission: The effect of pH during and post synthesis. J. Phys. Chem. C 123: 6010-6017. https://doi:10.1021/acs.jpcc.8b11716.
37. Chevrier DM, Thanthirige VD, Luo Z, Driscoll S, Cho P, MacDonald MA, Yao Q, Guda R, Xie J, Johnson ER, Chatt A, Zheng N, Zhang P (2018) Structure and formation of highly luminescent protein-stabilized gold clusters. Chem. Sci. 9: 2782-2790. https://doi:10.1039/C7SC05086K.
38. Pyo K, Thanthirige VD, Kwak K, Pandurangan P, Ramakrishna G, Lee D (2015) Ultrabright luminescence from gold nanoclusters: Rigidifying the Au(I)–thiolate shell. J. Am. Chem. Soc. 137: 8244-8250. https://doi:10.1021/jacs.5b04210.
39. Wu Z, Du Y, Liu J, Yao Q, Chen T, Cao Y, Zhang H, Xie J (2019) Aurophilic interactions in the self-assembly of gold nanoclusters into nanoribbons with enhanced luminescence. Angew. Chem. Int. Ed.

58: 8139-8144. https://doi:10.1002/anie.201903584.

40. Zhang W, Lin D, Wang H, Li J, Nienhaus GU, Su Z, Wei G, Shang L (2017) Supramolecular self-assembly bioinspired synthesis of luminescent gold nanocluster-embedded peptide nanofibers for temperature sensing and cellular imaging. Bioconjugate Chem. 28: 2224-2229. https://doi:10.1021/acs.bioconjchem.7b00312.
41. Kluz M, Nieznańska H, Dec R, Dzięcielewski I, Niżyński B, Ścibisz G, Puławski W, Staszczak G, Klein E, Smalc-Koziorowska J, Dzwolak W (2019) Revisiting the conformational state of albumin conjugated to gold nanoclusters: A self-assembly pathway to giant superstructures unraveled. PLoS One 14: e0218975. https://doi:10.1371/journal.pone.0218975.
42. Francos MAE, Badía-Laíño R, Díaz-García ME (2015) Fluorescence sensitization of gold-glutathione nanoclusters by aqueous solutions of sodium and potassium ions. Microchim. Acta 182: 1591-1598. https://doi:10.1007/s00604-015-1475-y.
43. Wei Y, Luan W, Gao F, Hou X (2019) Supramolecules-guided synthesis of brightly near-infrared Au22 nanoclusters with aggregation-induced emission for bioimaging. Part. Part. Syst. Charact. 36: 1900314. https://doi:10.1002/ppsc.201900314.

Figures

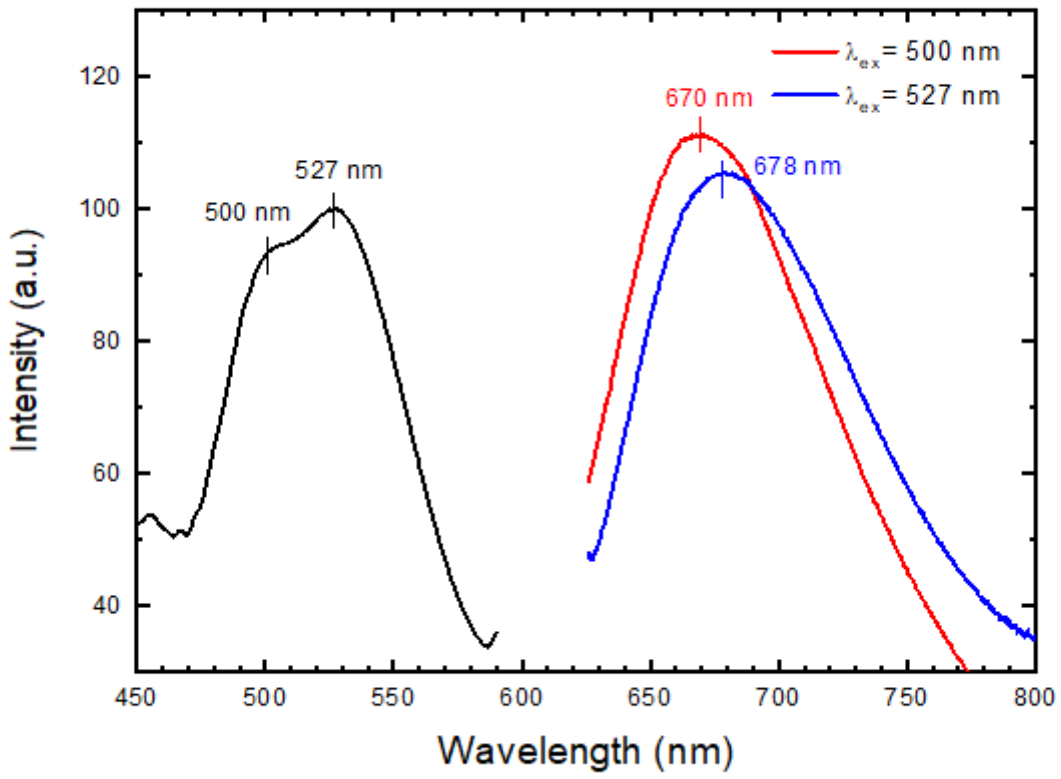

Figure 1

Photoexcitation and emission spectra of BSA-rAuNCs acquired with a commercial spectrofluorometer.

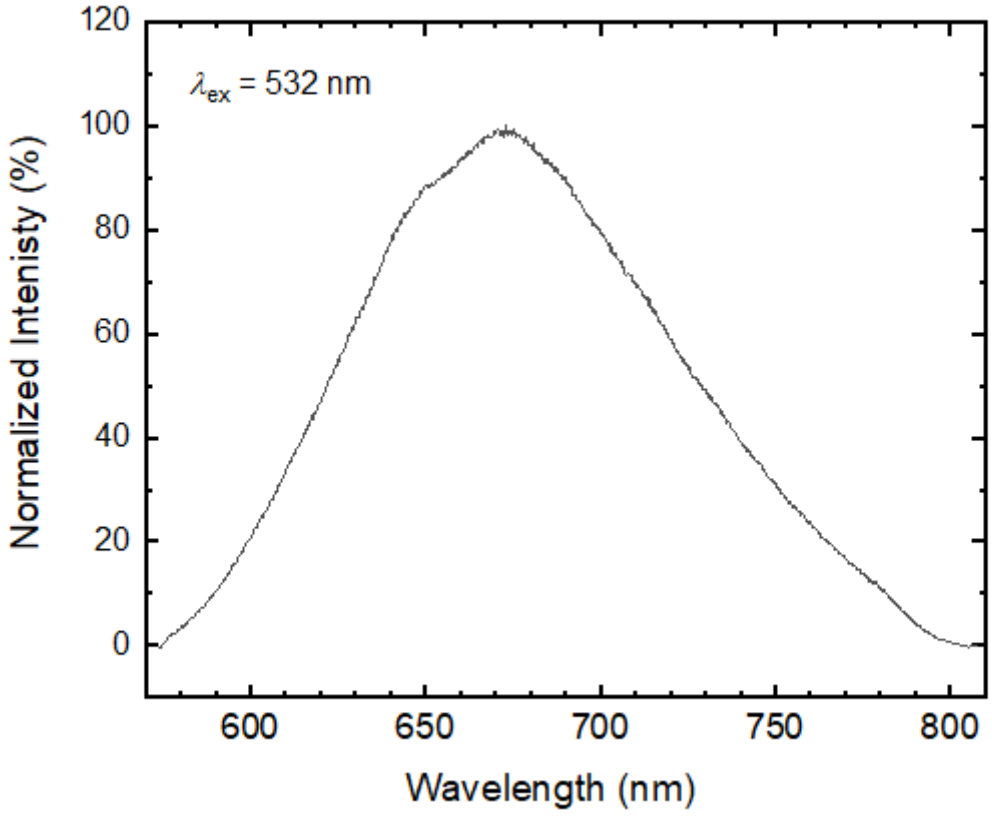

Figure 2

Normalized emission spectrum of BSA-rAuNCs in water, acquired with the custom-built fluorescence set-up.

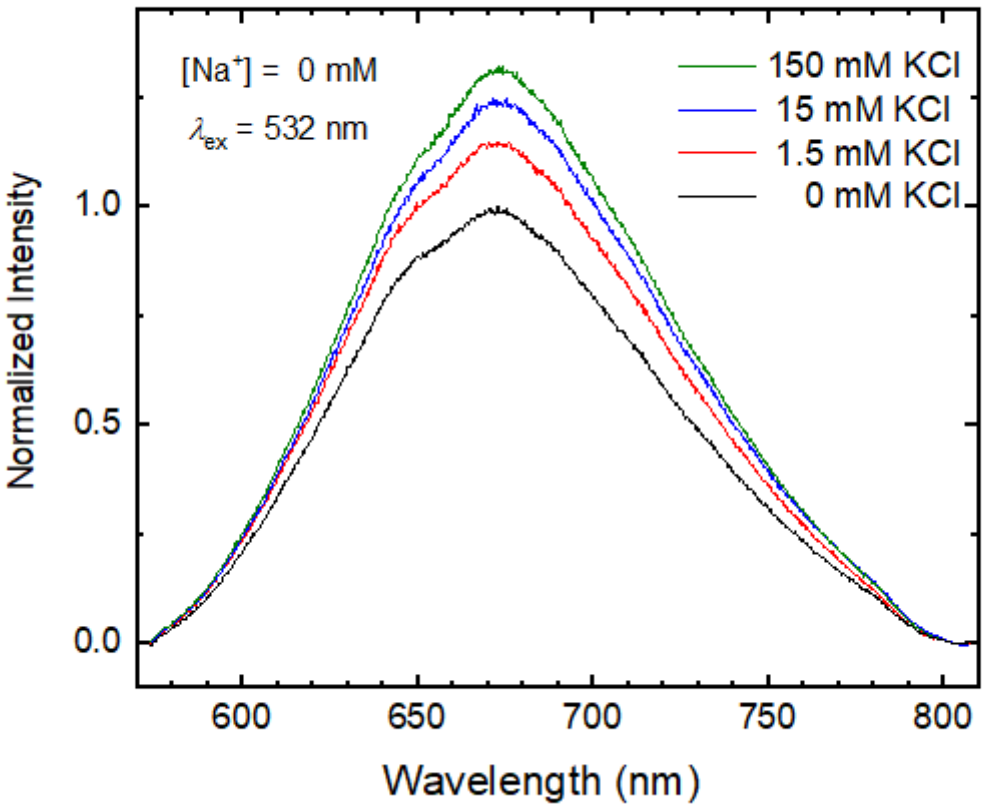

Figure 3

Emission spectra of BSA-rAuNCs in water, in the presence of KCl. Spectrum at 0 mM KCl was used for normalization.

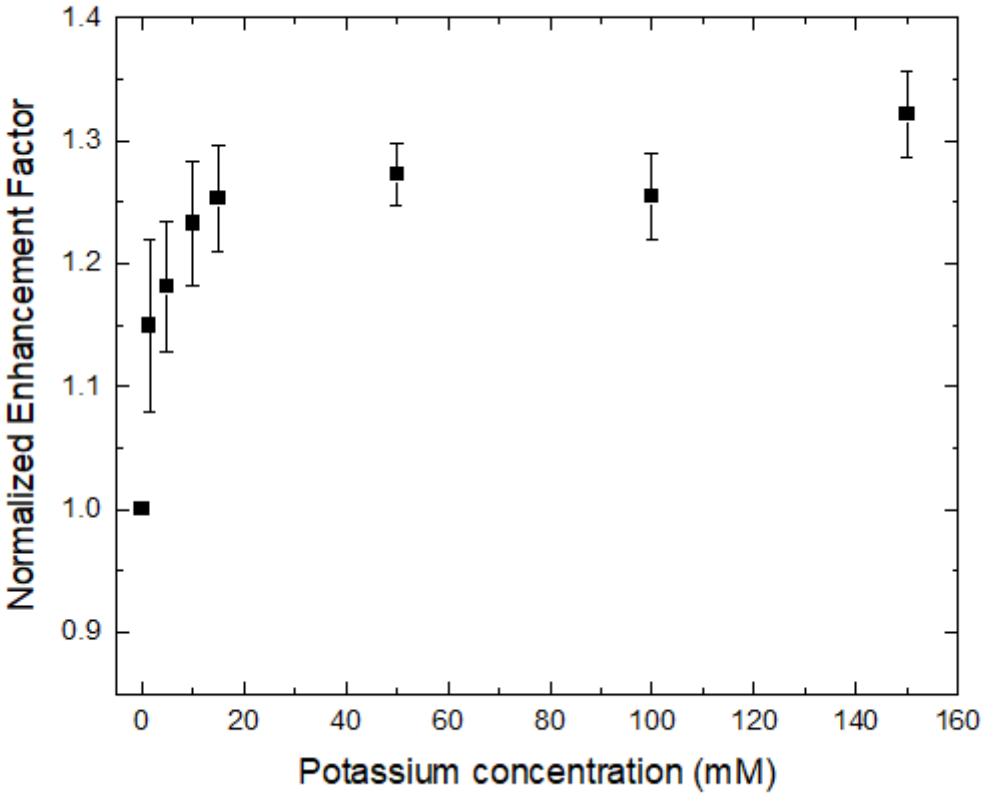

Figure 4

Normalized enhancement factor of BSA-rAuNCs as a function of KCl concentration.

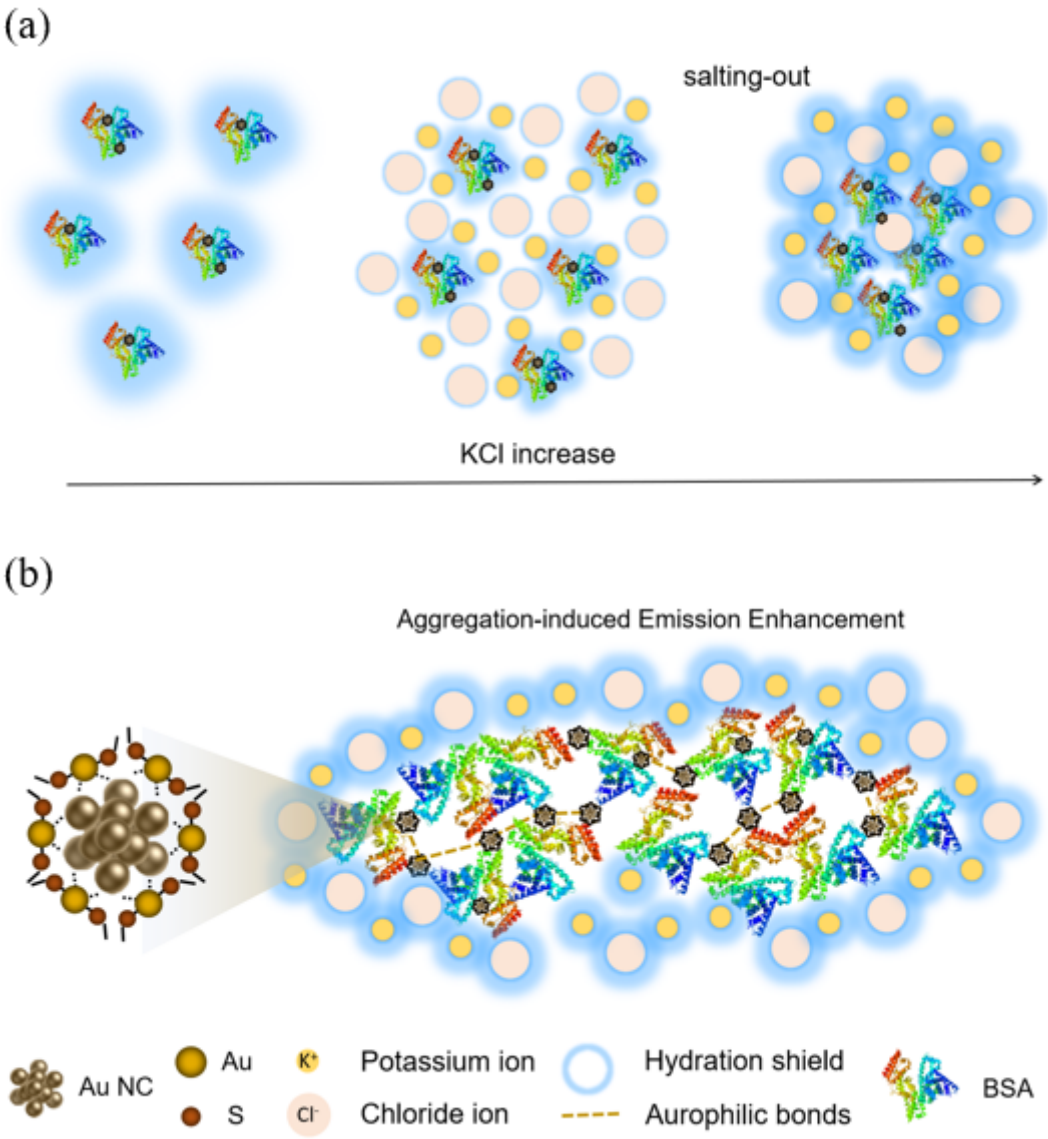

Figure 5

Schematic presentation of (a) hydrodynamic size increase as concentration of KCl increases (b) a final assemble where the aurophilic bonds form.

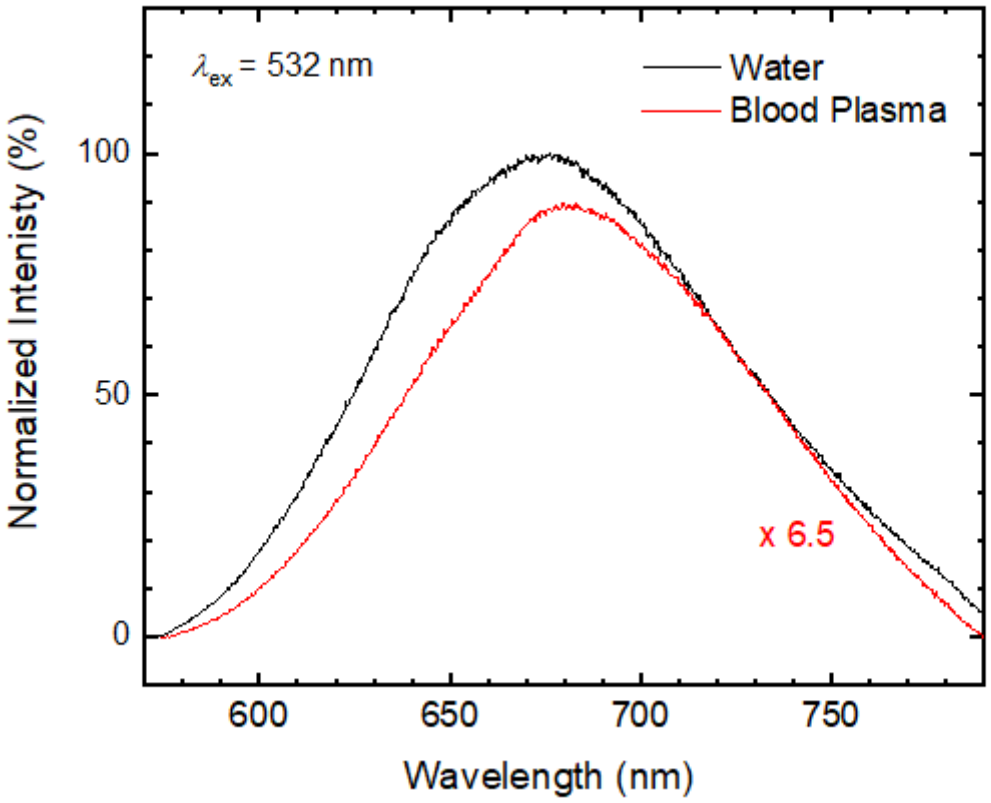

Figure 6

Emission spectra of BSA-rAuNCs in bovine blood plasma, acquired with the custom-built fluorescence set-up. The black line shows the spectrum in water which was used for normalization.

Supplementary Files

This is a list of supplementary files associated with this preprint. Click to download.

- HidayatSupportingInformationRzeznicka211128.docx